# Force-dependent remodeling of cytoplasmic ZO-1 condensates contributes to cell-cell adhesion through enhancing tight junctions

Noriyuki Kinoshita*[1,3], Takamasa S. Yamamoto[1], Naoko Yasue[1], Chiyo Takagi[1], Toshihiko Fujimori[2,3], and Naoto Ueno*[1,3,4,5]

Running title: Force-dependent remodeling of ZO-1 by phase separation

1: Division of Morphogenesis, Department of Developmental Biology, National Institute for Basic Biology, 38 Nishigonaka, Myodaiji, Okazaki, Aichi, 444-8585, Japan

2: Division of Embryology, Department of Developmental Biology, National Institute for Basic Biology, 5-1 Higashiyama, Myodaiji, Okazaki, Aichi 444-8787, Japan

3: School of Life Science, SOKENDAI (The Graduate University for Advanced Studies), Okazaki, Aichi, 444-8585, Japan

4. Unit of Quantitative and Imaging Biology, International Research Collaboration Center, National Institutes of Natural Sciences, 38 Nishigonaka, Myodaiji, Okazaki, Aichi, 444-8585, Japan

5: Lead Contact

* corresponding authors:
nueno@nibb.ac.jp (NU), nkinoshi@nibb.ac.jp (NK.)

**Summary (150 words)**

The physiological importance of biomolecular condensates is widely recognized, but how it is controlled in time and space during development is largely unknown. Here we show that a tight junction protein ZO-1 forms cytoplasmic condensates in the trophectoderm (TE) of the mouse embryo before E4.0. These disappear via dissolution, and ZO-1 accumulates at the cell junction as the blastocyst cavity grows and internal pressure on TE cells increases. In contrast, this dissolution was less evident in TE cells attached to the inner cell mass since they receive weaker tensile forces. Furthermore, analyses using MDCK cells demonstrated that the ZO-1 condensates are generated and maintained by liquid-liquid phase separation. Our study also highlights that the dynamics of these condensates depends on the physical environment via an interaction between ZO-1 and F-actin. We propose that the force-dependent regulation of ZO-1 condensation contributes to the establishment of robust cell-cell adhesion during early development.

**Keywords**

Cell-to-cell adhesion, ZO-1, tight junction, mechanical force, mouse development, condensate, liquid-liquid phase separation (LLPS), intrinsically disordered region (IDR).

## Introduction

Mechanical forces are generated at different times and in different tissues during the development of organisms due to, among other factors, dynamic movements and changes in the shapes of cells and tissues (Bodor et al., 2020), growth of cell masses by proliferation (Godard and Heisenberg, 2019), the removal of cells by apoptosis (Teng et al., 2017), luminal pressure (Chan et al., 2019), and shear stress of body fluids such as blood (Paolini and Abdelilah-Seyfried, 2018). All of these forces can contribute to the morphogenesis of organs through mechanochemical feedback mechanisms (Hannezo and Heisenberg, 2019). Although the presence and physiological importance of such forces have long been implicated in the homeostasis and morphogenesis of living organisms (Hallou and Brunet, 2020; Thompson, 1917), how cells sense and respond to these forces is not fully understood at the molecular level. This study demonstrates that mechanical forces control the remodeling of ZO-1 through the regulation of liquid-liquid phase separation (LLPS). ZO-1 is a tight junction (TJ) protein that links transmembrane proteins, such as claudins, to the actin cytoskeleton (Otani and Furuse, 2020), whereby mechanical forces loaded on the TJ change the conformation of ZO-1 (Haas et al., 2020; Spadaro et al., 2017).

LLPS is a physical process that facilitates the demixing of proteins via protein condensation and forms membrane-less organelles (Banani et al., 2017; Brangwynne, 2013; Shin and Brangwynne, 2017). Many components of LLPS condensates possess intrinsically disordered regions (IDRs) that are involved in weak multivalent molecular interactions (Kedersha et al., 2013). Compartmentalization of functional proteins by LLPS has been implicated in many cellular phenomena, such as transcription (Hnisz et al., 2017), stress response (Protter and Parker, 2016), neuronal development (Wu et al., 2020), and cell division (Ong and Torres, 2020). LLPS also regulates the formation of TJs. Recent studies revealed that ZO-1 is regulated by LLPS in mammalian tissue culture cells (Beutel et al., 2019) and zebrafish embryos (Schwayer et al., 2019). Beutel et al. (2019) demonstrated that ZO-1 formed membrane-attached compartments via phase separation, which is required to assemble functional TJs. Schwayer et al. (2019) found that non-junctional ZO-1 formed clusters and was transported towards TJs with the actomyosin flow in gastrulating zebrafish embryos.

TJs as well as adherens junctions (AJs) of epithelial cells in animal embryos are essential structures for orchestrated cell and tissue movements during normal

development. Our previous study using *Xenopus laevis* embryos demonstrated that cell junction-related proteins, including ZO-1, are highly phosphorylated immediately after applying mechanical forces, either by centrifugation or compression (Hashimoto et al., 2019). Furthermore, these forces induced mesenchymal-epithelial transition (MET)-like responses, enhancing cell-to-cell adhesiveness by accumulating cell junctional components, such as ZO-1, at cell-cell junctions, which is reminiscent of cellular events during *Xenopus* gastrulation (Kinoshita et al., 2020). Furthermore, we found that ZO-1 forms cytoplasmic granules before gastrulation, and a mechanical force remodels these ZO-1 granules, leading to their accumulation at the TJs. Based on these observations and on previous reports that showed that ZO-1 could undergo LLPS in zebrafish embryos (Schwayer et al., 2019) and cultured cells (Beutel et al., 2019), we hypothesized that the ZO-1 LLPS is mechanically regulated, particularly by dynamic morphogenesis known as epiboly during gastrulation which imposes a tensile force on the ectoderm (Hernandez-Vega et al., 2017).

To extend the above study that employed *X. laevis* and to examine whether our working model could be extrapolated to other species such as mammals, we focused on mouse embryogenesis in this study. We obtained similar results to those with *Xenopus* and found cytoplasmic condensates of ZO-1 in the trophectoderm (TE) cells of early mouse embryos before E4.0, although the condensate disappeared upon stretching of TE cells due to expansion of the blastocyst cavity (blastocoel). When stretching of TE cells was inhibited, those cytoplasmic condensates did not disappear, supporting that ZO-1 condensate formation is regulated by mechanical forces. Furthermore, tissue culture experiments highlighted that the ZO-1 LLPS is sensitive to mechanical environments that affect F-actin dynamics. The present study reveals a previously unknown role of physical force that regulates the condensation of ZO-1, and contributes to the enhancement of cell-to-cell adhesion during early development.

## Results

### *ZO-1 condensates in early mouse embryos*

In our previous report (Kinoshita et al., 2020), we demonstrated that the stretch of ectodermal tissue in the *Xenopus* gastrula embryo induced a MET-like cellular response, including a reduction of cytoplasmic ZO-1 puncta and its accumulation at the cell junction. To examine whether the behavior of ZO-1 protein is conserved across species,

especially in mammals, we first immunostained mouse embryo ZO-1. We focused on E3.5 and E4.5 embryos since they hatch out of the zona pellucida (ZP) and their shape expands (Figure 1A). We fixed E3.5 and E4.5 embryos with paraformaldehyde and immunostained them with a ZO-1 antibody (Figure 1B). We found that the cells of E3.5 embryos showed a significantly higher number of ZO-1 puncta in the cytoplasm relative to E4.5 embryos. As development proceeded, the surface area of TE cells, particularly on the mural side, expanded and became thinner (Figure S1A and B). We found that the number of cytoplasmic ZO-1 puncta were reduced, and ZO-1 signal intensity at the plasma membrane in E4.5 embryos became higher than that of E3.5 embryos at the expense of their cytoplasmic pool (Figure 1C, D), without changing the total fluorescence intensity of the protein (Figure 1E left). Importantly, this change coincides well with the accumulation of F-actin at the cell cortex in E4.5 embryos (Figure 1B bottom and 1E right). This result suggests that the shuttling of ZO-1 protein from the cytoplasmic puncta to cell junctions occurs as development progressed. We observed a similar behavior of ZO-1 protein using ZO-1-GFP-expressing mouse embryos by live-imaging (Katsunuma et al., 2016) (Figures 1H, I, S2 and Video S1). These results are consistent with our previous finding, where ZO-1 puncta decreased in *Xenopus* ectodermal cells that were exposed to a higher tensile force (Hashimoto et al., 2019; Kinoshita et al., 2020).

Interestingly, however, in the polar TE cells attached to the inner cell mass (ICM) of E4.5 embryos, a significant number of condensates still remained in the cytoplasm (Figures 1B (B3) and F). Consistently, the fluorescent intensity of both anti-ZO-1 immunostaining and F-actin accumulation at the plasma membrane in polar TE cells was lower than in mural cells (Figure 1G). Since polar TE cells attach to the crowded ICM, these cells might be exposed to lower tensions.

***ZO-1 condensate is regulated by a force-dependent mechanism***

The dynamic behavior of ZO-1 protein led us to test whether the ZO-1 puncta in E3.5 embryos were formed by phase separation, by treating embryos with 1,6-hexanediol (HD), which is known to dissolve the LLPS assembly (Kroschwald et al., 2015; Shulga and Goldfarb, 2003). As shown in Figures 2A and B, 5% 1,6-HD reduced the number of particles within a few minutes, suggesting that phase separation formed these droplets in the mouse embryos.

We next examined whether the increased tensile force reduced ZO-1 puncta and

accumulated ZO-1 at the cell junction during hatching. It is known that developing mouse embryos from E4.0 to E4.5 experience a gradually increasing magnitude of luminal pressure due to expansion of the blastocyst cavity in the presence of the ZP (Chan et al., 2019; Leonavicius et al., 2018). Accordingly, the cortical tension of TE increases from E3.5 to E4.5 (Chan et al., 2019). In order to examine whether cortical tension regulates ZO-1 localization, we reduced actomyosin contractility by a ROCK inhibitor, H-1152 (Zenker et al., 2018). E4.5 embryos treated with H-1152 for 3 h shrunk (Figure 2C), suggesting that this treatment reduced tension. In these embryos, the number of cytoplasmic ZO-1 particles increased (Figures 2D and E). Accordingly, junctional ZO-1 in the treated embryos became discontinuous on the cell membrane, but more uniformly distributed in control embryos (Figure 2C).

To further confirm that the disappearance of ZO-1 condensates from the cytoplasm is dependent on a mechanical force (inner hydraulic pressure of blastocyst cavity), using ouabain, we inhibited $Na^+/K^+$ ATPase, which promoted the influx of water and therefore increased the volume of the blastocyst cavity (Figure 2F). In these ouabain-treated embryos, a number of ZO-1 condensates were retained in the cytoplasm of mural cells of E4.5 embryos (Figures 2G and H), demonstrating that the cells released from this tension failed to trigger the dissolution of ZO-1 condensates.

Next, we mechanically reduced tension by releasing the blastocoel fluid of ZO-1-GFP-expressing embryos by piercing them with a glass needle. Immediately after they were pierced, embryos shrank, and membrane localization of ZO-1 was reduced, although it recovered within several hours after the wound site had healed and the embryo regained its original shape (Figures S3A, B, S4 and Video S2). Immunostaining with the anti-ZO-1 antibody confirmed that endogenous ZO-1 also behaved similarly, observing more cytoplasmic puncta in pierced E4.5 embryos than in control E4.5 embryos (Figure S3C-E). Together, these results suggest that the inner pressure of the growing blastocyst cavity increases the tensile force on TE cells in E4.5 embryos, thereby reducing the number and volume of ZO-1 puncta in the cytoplasm.

***LLPS forms ZO-1 droplets in MDCK cells***

In order to analyze the nature of the ZO-1 condensate in various cell environments, we performed a series of studies using canine MDCK cells. The results using mouse embryos suggested that tensile force on the TE cells negatively regulates ZO-1 phase separation. In

MDCK cells, increased substrate stiffness increases tension acting on ZO-1 (Haas et al., 2020). We thus examined whether substrate stiffness affects ZO-1 droplet formation. We plated MDCK cells on polyacrylamide gel substrates of different stiffness and immunostained ZO-1. As shown in Figures 3A and B, cells on soft substrates formed more cytoplasmic ZO-1 puncta than cells on rigid substrates. This result supports our proposed notion that sensing mechanical stimuli, including through focal adhesion, triggers the remodeling of ZO-1.

We also queried whether ZO-1 localization would change in an interaction with surrounding cells, which might affect the mechanical environment (Zhu et al., 2000). We grew MDCK cells to form islands in a culture dish and transfected a plasmid harboring human ZO-1 fused to GFP (GFP-ZO-1). It is notable that cells in the central region lost condensates while peripheral cells tended to have condensates (Figures 3C and D). This tendency was confirmed by immunofluorescence using the anti-ZO-1 antibody (Figure 3E). Quantitatively, cells in the forefront row (outermost layer) and the second row had 15 to 20 condensates per cell on average. In contrast, cells in the inner or central region had only a few condensates (Figure 3F). One feature that distinguished the inner cells from peripheral cells is that after cells reached confluency, the former adopted a polygonal shape and had higher densities than the latter. Consistently, we found that cells around the periphery of the islands had less claudin-1 at the cell junction than inner cells (Figure S5). These results suggest that the inner cells establish robust cell-to-cell contact by tight and adherens junctions, which are physically supported by the actin cytoskeleton, and an individual cell rigidly contacts with surrounding cells, resembling embryonic cells under a tensile force.

To further confirm that the ZO-1 droplets observed in MDCK cells are indeed the products of LLPS, we treated cells harboring GFP-ZO-1 droplets with digitonin, a cell-permeabilizing reagent that disrupts the equilibrium between a condensate and the cytoplasm. That treatment shrank the droplets within several minutes in MDCK cells (Figures 4A, B and Video S3). Furthermore, we performed FRAP analyses on GFP-ZO-1 droplets in MDCK cells (Figures 4C and D). The fluorescent signal of GFP-ZO-1 droplets recovered by almost 50% within 2 min. These results demonstrate that the ZO-1 puncta are droplet-like condensates produced by LLPS and are in equilibrium with the cytoplasm.

Junctional ZO-1 is also assembled by the LLPS, and ZO-1 LLPS is required for the

assembly of functional tight junctions (Beutel et al., 2019). We thus conducted a FRAP assay using inner cells with junctional ZO-1 (Figures 4E and F) and found that ZO-1 at the junction showed a similar recovery rate. These results indicate that both ZO-1 in the cytoplasmic droplets and ZO-1 at the junction are liquid-like condensates and that ZO-1 changes its localization depending on the cellular environment.

***Cell-cell interaction regulates ZO-1 droplet formation***

Our finding that peripheral cells have more droplets than inner cells suggested that robust cell-to-cell contact negatively regulates ZO-1 LLPS. To verify this idea, we reduced cell-to-cell contact by treating MDCK cells expressing GFP-ZO-1 with PBS containing trypsin-EDTA. As expected, when trypsin-EDTA solution was added, ZO-1 detached from the cell membrane and formed puncta as cell-to-cell contact was lost (Figure 5G and Video S4). We performed a FRAP assay on puncta produced in the trypsin-EDTA treatment (Figures 4H and I) and observed the rapid recovery of fluorescence (60% recovery within 3 min), suggesting that the puncta were generated by LLPS.

The robustness of cell-to-cell contact was also examined by laser ablation (Kinoshita et al., 2020; Yamamoto et al., 2021). MDCK cells were grown so that they formed islands in one culture dish. After the GFP-ZO-1 expression plasmid was transfected, cells were irradiated with laser light. When cells inside the islands were irradiated at the cell junction, cells remained stable after irradiation due to cell-to-cell contact with neighboring cells (Figures S6A, C and Video S5). When peripherally-located cells with ZO-1 puncta were irradiated, those cells immediately erupted and disappeared after irradiation (Figures S6B, C, and Video S6), suggesting that those cells are weakly attached to surrounding cells. This is consistent with our result that showed that claudin-1 accumulated more at the cell junction in inner-located cells than in peripheral cells (Figure S5). These results suggest that in MDCK cells, the formation of ZO-1 condensate is negatively associated with the establishment of robust cell-to-cell contact.

***ZO-1 forms cytoplasmic condensates in migrating cells during wound healing***

To further examine whether cell-to-cell contact negatively regulates ZO-1 condensate formation in the cytoplasm of MDCK cells, we conducted a wound-healing assay using GFP-ZO-1–expressing cells (Figure 5A and Video S7). Initially, 80% of the cells had few condensates in a confluent cell sheet. After scratching, cells started to migrate toward the

wound site, forming ZO-1 droplets. We found that cells closer to the wound site formed droplets more frequently ("0-40 μm" in Figure 5B) than cells located further away ("40-80" and "80-200 μm"). This suggests that cells may sense the wounding stimulus, forming ZO-1 droplets. However, we also found that most of the cells in this assay formed ZO-1 droplets several hours after wounding, and we could not detect a correlation between the time of droplet formation and distance from the wound site (R = 0.076 in Figure 5C). In this system, ZO-1 droplet formation could be involved in drastic reorganization of the cytoskeleton and cell adhesion.

By longer incubation in this assay, cells migrating from both sides eventually met in the middle of the gap, reestablishing a new cell-to-cell interaction. During this process, ZO-1 droplets disappeared and accumulated at the cell junction (Figure S7 and Video S8). These results indicate that ZO-1 condensates shuttle between cytoplasmic droplets and the cell junction, depending on cell-to-cell interaction.

The FRAP assay revealed that the fluorescent signals of GFP-ZO-1 condensates that had formed during the wound-healing assay recovered to about 40% within 5 min, suggesting that these condensates were formed by LLPS (Figures 5D, E, Videos S9, and S10). This result again indicates that the formation of ZO-1 condensates is regulated by extracellular environments such as cell-to-cell contact.

In the wound-healing assay, we found that the distribution and intensity of F-actin were different between inner cells and edge cells. As shown in Figures 5F and G, cortical F-actin was well-developed in the non-migrating polygonal cells with junctional ZO-1 ("inner" cells in Figure 5F). In contrast, migrating cells around the wound site, which formed ZO-1 droplets, had reduced cortical actin (Figure 5G). This association between ZO-1 and F-actin is consistent with our previous finding in which the application of force to *Xenopus* embryonic cells induced a MET-like response, including the accumulation of cortical F-actin, and reduced ZO-1 condensates as cell-to-cell junctions were enhanced (Hashimoto et al., 2019 ; Kinoshita et al., 2020).

***Interaction with F-actin regulates ZO-1 phase separation***

We further investigated the relationship between ZO-1 phase separation and F-actin organization by expressing GFP-ZO-1 in non-confluent *Xenopus* A6 cells. In A6 cells, GFP-ZO-1 localized mostly in the cell periphery and colocalized with F-actin bundles (Figure 6A). After cells were treated with latrunculin B, a potent inhibitor of actin

polymerization, ZO-1 granules rapidly emerged in the cytoplasm, which disappeared soon after washing out the drug (Figure 6B and Video S11). These results suggest that the ZO-1 granules, which were highly mobile in the FRAP assay (Figure 6C and D), are negatively regulated by the interaction with F-actin in A6 cells. We also treated confluent A6 cells expressing GFP-ZO-1 with latrunculin B. In contrast to non-confluent A6 cells, GFP-ZO-1 in confluent A6 cells did not form cytoplasmic droplets and ZO-1 stayed at cell junctions (Figure S8). ZO-1 is known to interact with F-actin and TJ proteins such as claudins (Otani and Furuse, 2020). Mature tight junctions might sustain contact with ZO-1 even after F-actin disruption.

In the case of MDCK cells, latrunculin treatment did not increase cytoplasmic droplets, as was reported by Beutel et al. (2019). Thus, we attempted to increase F-actin with jasplakinolide, which stabilizes F-actin (Crews et al., 1986; Shurety et al., 1998; Zabriskie et al., 1986). We found that in MDCK cells with GFP-ZO-1 droplets, jasplakinolide reduced the intensity of GFP-ZO-1 droplets, and GFP-ZO-1 localized to stabilized F-actin (Figure S9 and Video S12). These results suggest that, in both A6 cells and MDCK cells, F-actin suppresses cytoplasmic ZO-1 condensation.

To understand the F-actin-driven mechanism, we constructed GFP-ZO-1ΔABD (Figure 6E), which lacks the actin-binding domain (ABD) (Fanning et al., 2002), and expressed it in A6 cells. As shown in Figure 6F, GFP-ZO-1ΔABD formed droplets with a smooth surface. This suggests that cytoplasmic droplet formation is restricted by the binding of ZO-1 to F-actin (Beutel et al., 2019; Schwayer et al., 2019) and that GFP-ZO-1ΔABD lost its capacity for the interaction. Supporting this notion, co-expression with a red fluorescent protein fused to F-actin-binding peptides, Lifeact, Utrophin, and the actin-binding domain of Moesin (MoesinABD), similarly induced condensates that were indistinguishable from those induced by GFP-ZO-1ΔABD (Figure S10A). It is likely that the expression of these actin-binding proteins competes with the binding of F-actin to ZO-1.

We also observed that the MoesinABD-induced ZO-1 condensates moved dynamically, sometimes fused and underwent fission (Figure S10B and Video S13), reminiscent of typical liquid droplets. In addition, the size of these droplets was rapidly reduced by cell permeabilization following digitonin treatment (Figure S10C and Video S14) and exhibited a rapid recovery of fluorescence in the FRAP assay (Figure S10D). These results confirm that these cytoplasmic droplets are formed by phase separation.

***The C-terminal intrinsically disordered region is required for ZO-1 phase separation***

It is known that intrinsically disordered regions (IDRs) are required for proteins to undergo phase separation (Kato et al., 2012; Li et al., 2012). Four IDRs were predicted in human ZO-1 (Figure S11A) using the Protein DisOrder prediction System (https://prdos.hgc.jp/cgi-bin/top.cgi) (Ishida and Kinoshita, 2007). In order to address which IDR is critical for ZO-1 in A6 cells, we expressed a series of deletion mutants (Figure S11B). As a positive control, we expressed GFP-ZO1-ΔABD and confirmed that it formed droplets. Then, we deleted IDR1, IDR2, and IDR3, which reside in the N-terminal half, from GFP-ZO1-ΔABD (GFP-ZO1-ΔABD-ΔIDR123). When GFP-ZO1-ΔABD-ΔIDR123 was expressed, it also formed droplets (Figure S11C), indicating that these regions are not required for phase separation in A6 cells. In contrast, deletion of the C-terminal IDR4 (GFP-ZO1-ΔABD-ΔIDR4) abolished ZO-1 droplets, and GFP-ZO1-ΔABD-ΔIDR4 became dispersed in the cytoplasm. The result demonstrates that IDR4 is critical for cytoplasmic liquid droplet formation by LLPS. Since the actin-binding domain overlaps with IDR4, it is possible that F-actin binding may affect the LLPS-inducing activity of IDR4.

## Discussion

Our present study using mouse embryos as well as cultured cells, together with a previous study that employed *Xenopus* embryos (Kinoshita et al., 2020), indicates that similar mechanisms may govern cellular responses to mechanical forces across species. Since embryonic tissues, as well as some adult tissues, are constantly exposed to various forces, and because ZO-1 is a structurally conserved protein among species, we propose that this mechanism may be employed to maintain the robustness and integrity of tissues against various forces in general, and might also have been an evolutionary innovation when multicellular animal species such as placozoa emerged (Gonzalez-Mariscal et al., 2011). Although our previous study using *Xenopus* embryos identified that the function of the FGF receptor is essential for the force-induced pathway, it also suggested that FGF ligands are not required for signal activation, shedding light onto the as yet unrevealed activation mechanisms for FGFRs and other receptor tyrosine kinases (RTKs) by force. In fact, the epidermal growth factor receptor (EGFR), which is an upstream RTK for Erk, was implicated in the mechanical force-dependent activation of Erk in the collective

migration of wound-healing cells (Hino et al., 2020). In both cases, cytoskeletal remodeling by tensile forces appears to trigger these pathways, supporting the idea that mechanoresponsive signaling pathways may be highly conserved.

Interestingly, our present study using cultured cells demonstrated that the efficacy of ZO-1 condensation as droplets largely depends on cell type. In MDCK cells, cytoplasmic ZO-1 condensates are formed when they are cultured sparsely, or cell-to-cell interaction is weakened, for example, at the periphery of the islands, during the wound-healing process, or by trypsin/EDTA treatment. In contrast, in cells with a robust cell-to-cell interaction, ZO-1 condensates appear to be localized at the cell junction. In the case of A6 cells, blocking the interaction between ZO-1 and F-actin induces ZO-1 droplet formation, suggesting that ZO-1 droplet formation is negatively regulated by the interaction with F-actin. This suggests that the difference in the amount or dynamics of F-actin may distinguish these two cell types.

It is tempting to speculate that Erk might regulate F-actin polymerization through small G proteins such as GEF-H1 and its downstream target RhoA (Fujishiro et al., 2008; Itoh et al., 2014; Ren et al., 1998). Recently, Haas et al. (2020) reported that substrate stiffness regulates GEF-H1, thereby increasing tension, by acting on ZO-1. Since we reported in this study that substrate stiffness changes ZO-1 droplet formation, it would be intriguing to investigate whether the GEF-H1 pathway is involved in the regulation of ZO-1 phase separation. Second, as described above, it was reported that Erk is activated in collectively migrating MDCK cells by EGFR and regulates F-actin organization and cellular contraction (Hino et al., 2020). It is also possible that the cascade of phosphorylation initiated by RTKs might eventually result in the remodeling of F-actin and ZO-1 localization.

It has been reported that the assembly of ZO-1 at the cell junction is also driven by phase separation (Beutel et al., 2019). We also confirmed that both the cell junction and the cytoplasmic ZO-1 granules show typical characteristics of phase-separated condensates. This suggests that ZO-1 localization may be dynamically switched, depending on the mechanical environments, and that F-actin plays a key role in the switching in A6 cells. We also mapped the region essential for cytoplasmic granule formation to the fourth IDR (IDR4 in Figure S4). As IDR4 covers the actin-binding domain, the interaction with F-actin may directly affect its phase separation. It has been reported that F-actin binding to ZO-1 induces its conformational change (Spadaro et al.,

2017). Such structural changes may regulate the phase separation of IDR4 to form cytoplasmic droplets. Beutel et al. (2019) demonstrated that the PDZ-SH3-GuK domain in ZO-1 plays an essential role in phase separation at the cell junction. Since ZO-1 is a scaffold protein that interacts with many proteins (Fanning and Anderson, 2009), such a protein-protein interaction may also change the state of phase separation, resulting in differences between the cytoplasmic and junctional forms of condensates. Investigating the precise molecular mechanisms that could explain the two distinct states of ZO-1 will be important.

It has been reported that tension mediates the remodeling of cell junctions (Ito et al., 2017). Phase separation of ZO-1 may be directly involved in this regulatory system. In this scenario, LLPS may act as an on-demand ON/OFF switch of ZO-1 supply to the cell membrane from the cytoplasm, and this mechanism may be shared and employed by multicellular animal species. Therefore, its evolutionary origin is an intriguing problem worth studying in the future.

ZO-1 is implicated in various pathologies, including cancer. Particularly, in EMT, the loss of cell-to-cell adhesion is known to drive the progress and metastasis of cancer. It is also known that in neuronal cells, some condensates which contain proteins, such as the RNA-binding protein FUS (Murray et al., 2017) and tau implicated in Alzheimer's disease (Wegmann et al., 2018), become aggregated depending possibly on their concentrations, sometime after their formation and/or their chemical modifications. Those proteins are irreversibly aggregated and become dysfunctional, attenuating the neuronal activity of the cells. Collectively considering these observations, we speculate that impairment of the normal regulation of the LLPS of ZO-1 due to changes in intracellular or extracellular conditions could be a possible cause of cancer pathology. Therefore, in addition to embryogenesis, investigating the behavior of ZO-1 in adult tissues, especially in pathological conditions, would deepen our understanding of the physiological significance of the ZO-1 reservoir in cells.

**Limitations of this study**

We proposed in this paper that F-actin remodeling is one of the key factors to regulate ZO-1 shuttling between cytoplasmic and junctional condensates. However, particularly in MDCK cells, disruption of F-actin did not change junctional ZO-1 localization, suggesting that F-actin remodeling may not be sufficient for relocalizing ZO-1 in MDCK

cells. Since reducing cell-to-cell contact induced cytoplasmic ZO-1 droplet formation, there is likely to be a mechanism that releases junctional ZO-1 to the cytoplasm. The interactions with their junctional components, such as claudin, occludin, JAM-A, and cingulin (Fanning and Anderson, 2009; Haas et al., 2020; Vasileva et al., 2017) still to be clarified.

**Acknowledgments**

R26-ZO-1-GFP mice were provided by LARGE, BDR (accession # CDB026K), Japan. We thank Dr. Fumio Matsuzaki, RIKEN, for human ZO-1 cDNA, Dr. Makoto Suzuki, Hiroshima University, for the GFP-ZO-1/pCS2 construct, and Dr. Lance Davidson, University of Pittsburgh, for the mCherry-Utrophin construct. We thank Dr. Yuko Mimori-Kiyosue, RIKEN, for A6 cells and Dr. Mitsuru Nishita, Fukushima Medical University, and Dr. Kensaku Mizuno, Tohoku University, for MDCK I cells. thank the BioImaging Facility, Core Research Facilities of the National Institute for Biology (NIBB), for technical support for live imaging and FRAP analysis. We thank Dr. Akira Yamashita, NIBB, for advice in the statistical analyses. We also thank Dr. Nobuyuki Shiina, NIBB, and Dr. Michael Levine, Princeton University, for technical advice and valuable discussion on LLPS, and insightful comments on this work. This research was supported by JSPS KAKENHI 20K06663 to NK, JSPS KAKENHI 17H03689 and 16H06280 to TF, and MEXT KAKENHI 22127007, JSPS KAKENHI 15H05865 and 21H02493 to NU. TF and NU were also supported by JST CREST JPMJCR1654 and Joint Research of the Exploratory Research Center on Life and Living Systems (ExCELLS), respectively.

**Authors' Contributions**

N.K., T.S.Y., N.Y. and C.T. conducted experiments using tissue culture cells; T.F., N.K., and N.Y. conducted experiments using mouse embryos; N.K. analyzed the data and co-wrote the manuscript. N.U. supervised the research, reviewed the data and conclusions, and wrote the manuscript.

**Declaration of Interests**

The authors declare no competing interests.

444

## Figure legends

**Figure 1. Change of ZO-1 localization in hatching mouse embryos.**

**A**. Schematic diagram of the hatching process of the mouse embryo. At E3.5, the embryo is covered with the zona pellucida (ZP). During hatching, the embryo is enlarged with an expansion of the trophectoderm (TE), and emerges from the ZP. **B**. Immunofluorescence of mouse E3.5 and E4.5 embryos. Embryos were stained with an anti-ZO-1 antibody, Hoechst 33342, and Alexa Fluor 546 phalloidin. Scale bar, 20 μm. The inset in the E3.5 phalloidin image was acquired with higher laser power, demonstrating that the structure of cortical F-actin is formed at E3.5 even though the signal intensity was weaker than that in the E4.5 embryo. The right panels are enlarged images from the left panels indicated by the dashed squares B1, B2 and B3. **C**. The number of particles in one TE cell was counted. A total of 22 and 24 cells of six E3.5 and six E4.5 embryos, respectively, from two experiments (three embryos each) were analyzed. **D**. The signal intensity of ZO-1 at the cell periphery of the TE in E3.5 and E4.5 was quantified. Fifty cell boundaries in six E3.5 and six E4.5 embryos from two experiments (three embryos each) were analyzed. **E**. Fluorescence intensity of whole embryos stained with the anti-ZO-1 antibody and phalloidin was measured. For comparison, intensities were normalized by Hoechst staining intensity. Twelve E3.5 and 10 E4.5 embryos from two experiments (six E3.5 and five E4.5 embryos each) were analyzed. **F**. Comparison of ZO-1 particle numbers in polar and mural TE cells. The nuclear-dense inner cell mass (ICM) region was determined by Hoechst33342 staining. Here, ‘polar’ indicates TE attached to the ICM and ‘mural’ includes TE not attached to the ICM. The number of particles in one TE cell was counted. A total of 24 cells in mural and polar cells in four embryos from two experiments (two embryos each) were analyzed. **G**. Signal intensities of ZO-1 and phalloidin at the cell boundaries of the mural and polar TE were quantified. A total of 80 mural and 45 polar cell boundaries of four embryos from two experiments (two embryos each) were analyzed. **H**. Embryos from mice expressing ZO-1-GFP by GFP-knock-in were observed. After hatching (E4.5), junctional ZO-1 localization at cell boundaries became clear. Images were obtained from single Z planes using long-term live imaging. Images of other embryos are shown in Figures S2A and B. **I**. The fluorescence intensity around cell boundaries in ZO-1-GFP–expressing embryos was quantified. A total of 15 boundaries in five

embryos of each condition were analyzed. The average intensity values between – 0.5 and + 0.5 μm around the cell boundaries were statistically tested. n.s.: not significant. * $p < 0.01$ (Student's t-test). Scale bars, 20 μm. See also Figures S1, S2 and Video S1.

**Figure 2. ZO-1 droplets are formed by LLPS regulated by a force-dependent mechanism.**

**A**. Mouse E3.5 embryos were treated with 5% 1,6-hexanediol (1,6-HD). Images were analyzed by particle analysis (p.a.) in Image J software (right panels). **B**. The number of particles was counted. n = 5 (hexanediol) and 7 (control) embryos. Small dots with thin dotted lines indicate the number of particles in each embryo, Large dots indicate the average values and colored areas indicate standard deviations. ** $p < 0.05$ (Tukey-Kramer test). **C**. Embryos were obtained at E3.5, cultured for 24 h, then treated with 50 μM H-1152 for 3 h. Embryos were immunostained with the anti-ZO-1 antibody (left). **D** and **E**. The ratio of the particle area to the cytoplasm area in each cell. (D) and the number of particles per cell (E) of the mural TE cells were quantified using Image J software. A total of 80 cells in eight H-1152-treated embryos and 57 cells in six untreated embryos from two experiments (four treated and three control embryos each) were analyzed. **F**. Embryos were obtained at E3.5 and cultured for 24 h in the absence or presence of 0.3 mM ouabain (+Ob). Embryos were immunostained with the anti-ZO-1 antibody (left). **G** and **H**. The ratio of the particle area to the cytoplasm area in each cell. (G) and the number of particles per cell (H) of the mural TE cells were quantified using Image J software. A total of 24 cells in four Ob-treated and 24 cells in four untreated embryos from two experiments (two embryos each) were analyzed. * $p < 0.01$ (Student's t-test). Scale bars, 20 μm. See also Figures S3, S4 and Video S2.

**Figure 3. ZO-1 particle formation is regulated by extracellular environments.**

**A**. MDCK cells were grown on glass or on a polyacrylamide gel with 303, 138, and 19 kPa elasticity. **B**. The ratio of the particle area in each cell was counted by Particle Analysis in Image J software. A total of 40 cells each from two experiments (20 cells each) were analyzed on glass, 303, 138 and 19 kPa gel plates. * $p < 0.01$ (Mann-Whitney U test). **C** and **D**. GFP-ZO-1 was expressed in MDCK cells, forming islands. In cells located inside the islands (indicated by arrowheads), GFP-ZO-1 was localized mainly at the plasma membrane. In contrast, in cells at the periphery or

outside of the island (indicated by arrows), GFP-ZO-1 formed puncta. A total of 53 inner and 39 peripheral cells from two experiments (23 and 30 inner and 20 and 29 peripheral cells, respectively) were analyzed. Error bars, standard deviations. **E**. MDCK cells that formed an island were immunostained with the anti-ZO-1 antibody. Images were analyzed using particle analysis (p. a.) in Image J software. **F**. Cells in the island were divided into three groups based on their location, namely the first and second rows from the edge and the central region of the island. The number of particles in each cell was counted. For each condition, 40 cells from two experiments (20 cells each) were analyzed. * $p < 0.01$ (Student's *t*-test). See also Figure S5.

**Figure 4. Dynamics of ZO-1 puncta in MDCK cells.**

**A** and **B.** MDCK cells expressing GFP-ZO-1 were semi-permeabilized with 0.012% digitonin. The size of puncta was quantified with Image J software. n = 12 droplets in four cells. Scale bar, 20 μm. **C** - **F**. Fluorescent recovery after a photobleaching (FRAP) assay. **C** and **D**. The recovery of fluorescence of puncta was quantified. A total of 28 droplets in seven cells were analyzed. Scale bar, 20 μm. **E** and **F**. The recovery of junctional ZO-1 was quantified. A total of 30 cell junctions were analyzed. **G**. MDCK cells were treated with trypsin-EDTA solution. As cells lost their cell-cell contact and became spherical, ZO-1 detached from the plasma membrane and formed puncta. Scale bar, 20 μm. **H** and **I**. After trypsin-EDTA treatment for 60 min, droplets were analyzed by a FRAP assay. A total of 26 droplets in 11 cells were analyzed. Filled areas in the graphs, standard deviations. Scale bar, 5 μm. See also Figure S6 and Videos S3-6.

**Figure 5. Wound-healing assay using MDCK cells expressing GFP-ZO-1.**

**A**. The confluent cell sheet was scratched and observed. Immediately after scratching (0 h), the cell indicated by an arrowhead migrated toward the wound site. BF: bright field. Scale bar, 20 μm. **B**. The behavior of GFP-ZO-1 in the wound-healing assay was analyzed. The x axis consists of three groups of cells classified based on the distance from the wound site at the start time point of the assay. The y axis is the ratio of cells classified based on ZO-1 behavior: cells in which junctional ZO-1 formed droplets within 30 h (red bars, "junction to droplets"), cells whose ZO-1 stayed in the cell junction (blue bars, "junction"), and cells whose ZO-1 formed droplets from the beginning of the assay (gray bars, "droplets"). A total of 178 cells from two experiments

(81 and 97 cells, respectively) were analyzed. Error bars, standard deviations. **C**. Among 178 cells analyzed in Figure 6B, 93 cells that formed droplets during the assay were chosen and the distance from the wound site, as well as the time of droplet appearance, were plotted. R: correlation efficient. **D** and **E**. Wound-healing assay of MDCK cells expressing GFP-ZO-1 followed by a FRAP assay. Cells forming GFP-ZO-1 puncta in the wound-healing assay were subjected to the FRAP assay. A total of 29 droplets in 11 cells from three experiments were analyzed. Filled area, standard deviation. Scale bar, 20 μm. **F**. Inner and edge cells were fixed 10 h after scratching and stained with phalloidin. Arrow indicates the wound site: scale bar, 20 μm. **G**. The intensity of phalloidin fluorescence at the boundaries between each cell were measured. "n" is the number of measured cell boundaries. The data are from two experiments, 66 and 69 boundaries of inner cells and 45 and 57 boundaries of peripheral cells, respectively. * $p < 0.01$ (Mann-Whitney U test). See also Figure S7 and Videos S7-10.

**Figure 6. GFP-ZO-1 binding to F-actin in *Xenopus* A6 cells.**

**A**. GFP ZO-1 was transiently expressed in *Xenopus laevis* A6 kidney cells. Cells were fixed and stained with fluorescent phalloidin. **B**. A6 cells expressing GFP-ZO-1 were treated with 0.5 μM latrunculin B for 20 min, then washed out. **C**. A6 cells were treated with 0.5 μM latrunculin B for 30 min, then a FRAP assay was performed. Granules, indicated by arrowheads, were bleached. **D**. Recovery rate was quantified. A total of 14 droplets in six cells from three experiments (two cells each) were analyzed. Filled area, standard deviation. **E**. Domain structure of ZO-1 protein and expression constructs used here: GFP-tagged full-length human ZO-1 (GFP-ZO-1), actin-binding domain (ABD)-deletion mutant (GFP-ZO-1ΔABD). **F**. Localization of GFP-ZO-1 and GFP-ZO-1ΔABD. Scale bars, 20 μm. See also Figures S8-11 and Videos S11-14.

## STAR★Methods

### KEY RESOURCES TABLE

| REAGENT or RESOURCE | SOURCE | IDENTIFIER |
|---|---|---|
| Antibodies | | |
| anti-ZO-1 antibody | Thermo Fisher Scientific | cat. # 33-9100; RRID:AB_2533147 |
| goat anti-mouse IgG antibody, Alexa Fluor 488 | Thermo Fisher Scientific | cat. # A28175; RRID:AB_2536161 |
| anti-Claudin-1 antibody | Thermo Fisher Scientific | cat. # 51-9000 RRID: AB_2533916 |
| goat anti-rabbit IgG antibody, Alexa Fluor 555 | Thermo Fisher Scientific | cat. # A27039; RRID:AB_ 2536100 |
| Chemicals, Peptides, and Recombinant Proteins | | |
| Blocking One | Nacalai Tesque | cat.# 03953 |
| KSOM | Millipore | cat. # MR-106D |
| ouabain | Sigma-Aldrich | cat.# O3125 |
| Alexa Fluor 546 Phalloidin | Thermo Fisher Scientific | cat.# A22283; RRID:AB_2632953 |
| Hoechst 33342 | Thermo Fisher Scientific | cat.# H3570 |
| Lipofectamine 2000 | Invitrogen | cat. # 11668-027 |
| Effectene | Qiagen | cat. # 301425 |
| Latrunculin B | Enzo Life Science | cat. # BML-T110-0001 |
| digitonin | WAKO | cat. # 048-02124 |
| trypsin | Nacalai Tesque | cat # 35555-54 |
| (3-aminopropyl) triethoxysilane | Sigma-Aldrich | cat. # 440140 |
| Sulfo-SANPAH | Pierce | cat. # 22589 |
| 1.6-hexanediol | WAKO | cat. # 087-00432 |
| Experimental Models: Organisms/Strains | | |
| R26-ZO-1EGFP | RIKEN | accession # CDB026K |
| wild type ICR mice | Japan CREA | N/A |

| | | |
|---|---|---|
| Experimental Models: Cell Lines | | |
| MDCK I cells | Fujiwara et al. (2016) | N/A |
| A6 cells | Mimori-Kiyosue et al. (2007) | N/A |
| Recombinant DNA | | |
| human ZO-1 | Konno et al. (2008) | N/A |
| GFP-ZO-1/pCS2 | This paper | N/A |
| GFP-ZO-1ΔABD/pCS2 (Δ1151-1371) | This paper | N/A |
| GFP-ZO-1ΔABD-ΔIDR123/pCS2 (Δ114-118, Δ275-415, Δ588-627, Δ1151-1371) | This paper | N/A |
| GFP-ZO-1ΔIDR4/pCS2 (Δ858-1580) | This paper | N/A |
| GFP-ZO-1-PSG/pCS2 (424-794) | This paper | N/A |
| GFP-ZO-1ΔABDΔPSG/pCS2 (Δ424--794, Δ1151-1371) | This paper | N/A |
| Lifeact-RFP | Iioka et al. (2007) | N/A |
| RFP-MoesinABD | Iioka et al. (2004) | N/A |
| mCherry-Utrophin | Kim and Davidson (2013) | N/A |
| Software and Algorithms | | |
| Fiji | NIH | https://fiji.sc |
| Python 3.9 | Python Core Team | https://www.python.org |
| pandas | ver. 1.2.4 | http://pandas.pydata.org |
| seaborn | ver. 0.11.1 | https://seaborn.pydata.org |
| matplotlib | ver. 3.4.2 | https://matplotlib.org |
| scipy.stats | ver. 1.6.3 | https://docs.scipy.org/doc/scipy/reference/stats.html |
| statsmodels.stats.multicomp | ver. 0.13.1 | https://www.statsmodels.org/dev/index.html |

| | | |
|---|---|---|
| Andor IQ2 | Oxford Instruments | https://andor.oxinst.com/products/iq-live-cell-imaging-software/ |
| PrDOS (protein disorder prediction system) | (Ishida and Kinoshita, 2007) | http://prdos.hgc.jp/cgi-bin/top.cgi |

## Resource Availability

### Lead Contact

Further information and requests for resources and reagents should be directed to and will be fulfilled by the lead contact, Naoto Ueno (nueno@nibb.ac.jp).

### Materials Availability

All unique/stable reagents generated in this study are available from the lead contact with a completed Material Transfer Agreement.

### Data and code availability

• All data reported in this paper will be shared by the lead contact upon request.

• This paper does not report original code.

• Any additional information required to reanalyze the data reported in this paper is available from the lead contact upon request.

## Method details

### Mouse embryo collection

Animal care and experiments were conducted in accordance with the Guidelines of Animal Experimentation of the National Institutes for Natural Sciences. All animal experiments were approved by the Animal Research Committee of the National Institutes for Natural Sciences. Mice were maintained in a light- and temperature-controlled room using a 12 h light:12 h dark cycle at 23+/-2 °C.

Males of R26-ZO-1EGFP (Katsunuma et al., 2016) or wild-type ICR (Japan CREA) were mated with wild-type ICR females to obtain blastocysts. Preimplantation E3.5 embryos were flushed from uteri with KSOM (MR-106D, Millipore). Embryos were cultured in KSOM covered with mineral oil at 37 °C and 5% $CO_2$. Fluorescent signals were monitored using a confocal microscope (A1, Nikon) or a spinning disc confocal

microscope (CV1000, Yokogawa). For immunofluorescence, embryos were fixed at 4 °C in 4% paraformaldehyde (PFA) in PBS overnight. For ouabain treatment, 10 mM ouabain (cat. # O3125, Sigma-Aldrich) in DMSO was diluted to the indicated concentrations.

**Manipulation of mouse embryos**

To remove the zona pellucida, embryos were treated with Tyrode's solution (Bradley, 1987). Embryos were transferred to a drop of Tyrode's solution. The zona was removed typically within 1 min. Then, embryos were washed three times in KSOM. To pierce the mural trophectoderm, microinjection needles were made from a 1 mm diameter glass capillary (GD1, Narishige, Japan), the needle was set to a micromanipulator (Leica), and embryos were manually pierced with the needle.

For hexanediol treatment, 1,6-hexanediol (cat. # 087-00432, WAKO, Japan) was dissolved in water at 50% w/v, and a 1/10 volume was added to the culture medium. Fluorescent images were captured using CV1000 (Yokogawa, Japan).

**Immunofluorescence with mouse embryos**

Fixed embryos were washed three times with 1% bovine serum albumin (BSA) in PBS and then soaked in a blocking solution, 0.1% Triton X-100 in Blocking One (cat. # 03953, Nacalai-Tesque, Japan), for 1 h at room temperature. Embryos were then incubated in primary antibody solution containing an anti-ZO-1 antibody (cat. # 33-9100, Thermo Fisher Scientific) diluted 100-times in Blocking One at 4 °C overnight. After washing three times with the blocking solution, embryos were incubated in a secondary antibody solution containing 100-times diluted goat anti-mouse IgG antibody Alexa Flour 488 (cat. # A27185, Thermo Fisher Scientific), 100-times diluted Alexa Fluor 546 Phalloidin (cat. # A22283, Thermo Fisher Scientific), and 10 μg/ml Hoechst 33342 (cat. # H3570, Thermo Fisher Scientific) in Blocking One. Fluorescent signals were monitored using Nikon A1 or Leica SP8 confocal microscopes.

**Measurement of fluorescent intensities and particle analyses**

Fiji/Image J was used to measure fluorescent intensities. Particle analyses in Fiji/Image J were used to count particles and measure particle areas. A large mass signal in the

cavity was removed for quantitative analyses. Images were inverted and converted to an 8-bit type. Cytoplasmic regions were manually determined. The "Analyze Particles" program was run with the threshold signal value: 230, circularity: 0.3-1.0, and size: 3 - infinity.

To measure the line intensity plot across cell boundaries in ZO-1-GFP expressing mouse embryos, we selected pairs of clearly identified adjacent cells and drew a line between them, as shown in Figures S2 and S4. Then we conducted a line plot analysis in Image J software.

**GFP-ZO-1 expression constructs**

Human ZO-1 cDNA was a gift from Dr. Fumio Matsuzaki (Konno et al., 2008). EGFP-human ZO-1/pCS2 was constructed by Dr. Makoto Suzuki. ZO-1ΔABD lacks amino acid (aa) # 1151-1371. Lifeact-RFP is described in Iioka et al. (2007). MoesinABD is described in Iioka et al. (2004). The mCherry-Utrophin construct was a gift from Dr. Lance A. Davidson (Kim and Davidson, 2013).

**Cell culture and transfection of plasmids**

A6 cells, established from a normal *X. laevis* kidney, were a gift from Dr. Yuko Mimori-Kiyosue (Mimori-Kiyosue et al., 2007). A6 cells were grown at 24 °C without $CO_2$ in Leibovitz's L-15 medium (50% L-15 medium, 10% fetal bovine serum (FBS), 200 mg/l kanamycin). MDCK cells were a gift from Dr. Mitsuru Nishita and Dr. Kensaku Mizuno. MDCK cells were cultured in Dulbecco's modified Eagle medium (DMEM) containing 10% FBS. Transfection was conducted using Lipofectamine 2000 (Invitrogen # 11668-027) for MDCK cells and Effectene (Qiagen # 301425) for A6 cells following the manufacturers' instructions.

**Immunofluorescence of the tissue cultured cells**

Cells were fixed in 4% PFA in PBS at 4 °C overnight, washed with 0.1% Triton X-100 in PBS. Then the cells were soaked for 1 h at room temperature in Blocking One for blocking, followed by incubation in the primary antibody solution, a 100-times diluted anti-ZO-1 antibody (cat. # 33-9100, Thermo Fisher Scientific) in Blocking One at 4 °C overnight. After washing three times in Blocking One, cells were incubated in the secondary antibody solution containing 200-times diluted goat anti-mouse IgG antibody

Alexa Fluor 488 (cat. # A27185, Thermo Fisher Scientific) and 200-times diluted Alexa Fluor 546 Phalloidin (cat. # A22283, Thermo Fisher Scientific) in Blocking One at 4 °C overnight. After washing three times in PBS, cells were observed using a Leica SP8 confocal microscope.

For immunostaining of claudin-1, MDCK cells were fixed in cold methanol (-30 °C), or 10% TCA for 15 min at room temperature. The following procedure was the same as described above, except that we used 50-times diluted anti-claudin-1 antibodies (cat. # 51-9000, Thermo Fisher Scientific) and 200-times diluted goat anti-rabbit IgG antibody Alexa Fluor 555 (cat. # A27039, Thermo Fisher Scientific).

**Laser ablation**

Laser ablation was conducted using an Olympus IX 81 inverted microscope (20 × /0.70 NA dry objective lens), equipped with a spinning-disc confocal unit Yokogawa CSUX-1 and iXon3 897 EM-CCD camera (Andor), controlled with Andor IQ2 software. An N2 Micropoint laser (16 Hz, 365 nm, 2.0 μW, Photonic Instruments) was focused on the membrane at the apical cell membrane (Kinoshita *et al.*, 2020; Yamamoto *et al.*, 2021). Time-lapse images were acquired every 200 msec before and during the laser ablation process and analyzed with Fiji/Image J software.

**Fluorescence recovery after photobleaching (FRAP)**

FRAP assays in the tissue culture cells were conducted with a Leica SP8 confocal microscope and software equipped in the microscope operating system. Regions of interest (ROI) were bleached using a 488 nm laser. Pre-bleach and post-bleach images were acquired with a 488 nm laser. Fluorescence recovery of GFP-ZO-1 was monitored. Recovery data were background corrected and normalized to the ROI intensity before bleaching. A reference ROI outside the bleached area was processed in the same way.

**Observation of GFP-ZO-1 dynamics in the tissue culture cells**

For the wound-healing assay, MDCK cells almost confluently grown on a glass-bottom dish were transfected with GFP-ZO-1/pCS2. After one day, the cell layer was scratched with a Pipetman tip, incubated at 37 °C, 5% $CO_2$ in a stage-top incubator (cat. # STXG, Tokai HIT, Japan), and observed by a Leica SP8 confocal microscope.

For the latrunculin B treatment, 2.5 μM latrunculin B in the culture medium was

added to the culture dish of A6 cells transiently expressing GFP-ZO-1 so that the final concentration of latrunculin B was 0.5 μM. For the digitonin treatment, 0.06% digitonin in the culture medium was added to the culture dish so that the final concentration of digitonin was 0.012%. For the hyperosmolarity treatment of A6 cells, 10× PBS was added so that the concentration of PBS changed from 0.5× to 1.5×. Cells were observed at room temperature. For the trypsin-EDTA treatment, the culture medium of MDCK cells was replaced with PBS containing 0.05% trypsin and 1 mM EDTA.

**Preparation of polyacrylamide-based plates**

Glass bottom dishes (27-mm diameter, cat. # 3910-035, IWAKI, Japan) were treated with 2% (v/v) (3-aminopropyl) triethoxysilane (cat. # 440140 Sigma-Aldrich)/acetone. Air-dried plates were washed with sterilized water three times and dried at 50 °C for 2 h. 45 µl acrylamide solution was loaded, and then a 24-mm diameter coverslip was loaded onto the solution. After gelation, the coverslip was removed, and the surface of gelled polyacrylamide was washed with 50 mM HEPES (pH 8.5). 200 µl of 0.5 mg/ml Sulfo-SANPAH (cat. # 22589, Pierce) was loaded and irradiated with UV for 30 min using Stratalinker 2400 (Stratagene). Then, it was washed twice with 50 mM HEPES (pH 8.5), and 200 µl of 100 µg/ml fibronectin was loaded and incubated overnight at 4 °C. It was washed with the MDCK culture medium to block residual reactive groups, and cells were plated.

**Atomic force microscopy (AFM) measurements**

AFM measurements were conducted with a JPK Nanowizard Cellhesion 200 (JPK Instruments AG, Germany) fitted to an Axio Zoom V. 16 system (Zeiss). For a cantilever, CP-CONT-BSG-A (sQUBE, Germany) was used. Young’s modulus was calculated using JPK data processing software (Bruker). Measurement conditions were as follows: setpoint 50-200 nN, approach speed 2 µm/s, data rate 1000 Hz, measured spring constant 0.342 N/m.

**Quantification and statistical analysis**

Quantification was represented by the mean ± standard deviation. We performed two-tailed Student's t-test, Mann-Whitney U-test, and Tukey-Kramer test for the statistical analyses, as indicated in the figure legends, using Python scipy and

statsmodels packages. P values of less than 0.05 were regarded as statistically significant.

## Supplemental Video Legends

**Video S1.** Mouse embryos expressing ZO-1-GFP were flushed from uteri at one-day post-coitum and observed by time-lapse microscopy for 92 h. Related to Figure 1.

**Video S2.** Mouse E4.5 embryos expressing ZO-1-GFP were pierced by a glass needle and observed by time-lapse microscopy. Related to Figure 2 and S3.

**Video S3.** An MDCK cell expressing GFP-ZO-1 was treated with digitonin ("+digitonin" at 50 sec in the video) and imaged by time-lapse microscopy. Related to Figure 4.

**Video S4.** MDCK cells expressing GFP-ZO-1 were treated with a trypsin-EDTA solution. The video starts immediately after the treatment. Related to Figure 4.

**Video S5.** Laser ablation of MDCK cells expressing GFP-ZO-1 inside the island. The laser was irradiated at 4 sec at the membrane indicated by arrowheads. Related to Figure 3 and S6.

**Video S6.** Laser ablation of MDCK cells expressing GFP-ZO-1 at the periphery of the island. The laser was irradiated at 4 sec at the membrane indicated by the arrowhead. The cell erupted and disappeared immediately after irradiation. Related to Figure 3 and S6.

**Video S7.** A wound-healing assay of MDCK cells. A sheet of MDCK cells transfected with the GFP-ZO-1 construct was scratched and observed by time-lapse microscopy. Related to Figure 5.

**Video S8.** Shuttling GFP-ZO-1 between droplets and cell junction. In the wound-healing assay, GFP-ZO-1 was initially localized at the cell junction. When cells started migration, GFP-ZO1 formed droplets. When the wound gap was filled, and a new cell-cell interaction was established, GFP-ZO-1 was relocalized to the cell junction. Related to Figure 5.

**Video S9.** A wound-healing assay of MDCK cells, followed by a FRAP assay (1). A sheet of MDCK cells transfected with the GFP-ZO-1 construct was scratched and observed by time-lapse microscopy. The cell used for the following FRAP assay was indicated by an arrowhead in the last frame. Related to Figure 5.

**Video S10.** A wound-healing assay of MDCK cells, followed by a FRAP assay (2). The FRAP assay was conducted using a cell in Video S11, which formed ZO-1 puncta. Arrowhead indicates the granule bleached in the FRAP assay. Related to Figure 5.

**Video S11.** Latrunculin B treatment of an A6 cell co-expressing GFP-ZO-1 and RFP-MoesinABD. Related to Figure 6.

**Video S12.** Jasplakinolide treatment of an MDCK cell expressing GFP-ZO-1. Related to Figure 6.

**Video S13.** An A6 cell co-expressing GFP-ZO-1 and RFP-MoesinABD was imaged by time-lapse microscopy for 885 min. Related to Figure 6 and S10.

**Video S14.** A6 cells co-expressing GFP-ZO-1 and RFP-MoesinABD were treated with digitonin ("+digitonin" at 50 sec in the video) and imaged by time-lapse microscopy. Related to Figure 6 and S10.

## References


Banani, S.F., Lee, H.O., Hyman, A.A., and Rosen, M.K. (2017). Biomolecular condensates: organizers of cellular biochemistry. Nat Rev Mol Cell Biol *18*, 285-298. 10.1038/nrm.2017.7.

Beutel, O., Maraspini, R., Pombo-Garcia, K., Martin-Lemaitre, C., and Honigmann, A. (2019). Phase Separation of Zonula Occludens Proteins Drives Formation of Tight Junctions. Cell *179*, 923-936. 10.1016/j.cell.2019.10.011.

Bodor, D.L., Ponisch, W., Endres, R.G., and Paluch, E.K. (2020). Of Cell Shapes and Motion: The Physical Basis of Animal Cell Migration. Dev Cell *52*, 550-562. 10.1016/j.devcel.2020.02.013.

Bradley, A. (1987). Production and analysis of chimeric mice. In Teratocarcinoma and Embryonic Stem Cells, E.J. Robertson, ed. (IRL Press), pp. 113-151.

Brangwynne, C.P. (2013). Phase transitions and size scaling of membrane-less organelles. J Cell Biol *203*, 875-881. 10.1083/jcb.201308087.

Chan, C.J., Costanzo, M., Ruiz-Herrero, T., Monke, G., Petrie, R.J., Bergert, M., Diz-Munoz, A., Mahadevan, L., and Hiiragi, T. (2019). Hydraulic control of mammalian embryo size and cell fate. Nature *571*, 112-116. 10.1038/s41586-019-1309-x.

Crews, P., Manes, L.V., and Boehler, M. (1986). Jasplakinolide, a cyclodepsipeptide from the marine sponge, Jaspis sp. Tetrahedron letters *27*, 2797-2800.

Fanning, A.S., and Anderson, J.M. (2009). Zonula occludens-1 and -2 are cytosolic scaffolds that regulate the assembly of cellular junctions. Ann N Y Acad Sci *1165*, 113-120. 10.1111/j.1749-6632.2009.04440.x.

Fanning, A.S., Ma, T.Y., and Anderson, J.M. (2002). Isolation and functional characterization of the actin binding region in the tight junction protein ZO-1. FASEB J *16*, 1835-1837. 10.1096/fj.02-0121fje.

Fujishiro, S.H., Tanimura, S., Mure, S., Kashimoto, Y., Watanabe, K., and Kohno, M. (2008). ERK1/2 phosphorylate GEF-H1 to enhance its guanine nucleotide exchange activity toward RhoA. Biochemical and biophysical research communications *368*, 162-167. 10.1016/j.bbrc.2008.01.066.

Fujiwara, S., Ohashi, K., Mashiko, T., Kondo, H., and Mizuno, K. (2016). Interplay between Solo and keratin filaments is crucial for mechanical force-induced stress fiber reinforcement. Mol Biol Cell *27*, 954-966. 10.1091/mbc.E15-06-0417.

Godard, B.G., and Heisenberg, C.P. (2019). Cell division and tissue mechanics. Curr Opin Cell Biol *60*, 114-120. 10.1016/j.ceb.2019.05.007.

Gonzalez-Mariscal, L., Quiros, M., and Diaz-Coranguez, M. (2011). ZO proteins and redox-dependent processes. Antioxid Redox Signal *15*, 1235-1253. 10.1089/ars.2011.3913.

Haas, A.J., Zihni, C., Ruppel, A., Hartmann, C., Ebnet, K., Tada, M., Balda, M.S., and Matter, K. (2020). Interplay between Extracellular Matrix Stiffness and JAM-A Regulates Mechanical Load on ZO-1 and Tight Junction Assembly. Cell Rep *32*, 107924. 10.1016/j.celrep.2020.107924.

Hallou, A., and Brunet, T. (2020). On growth and force: mechanical forces in development. Development *147*, dev187302. 10.1242/dev.187302.

Hannezo, E., and Heisenberg, C.P. (2019). Mechanochemical Feedback Loops in Development and Disease. Cell *178*, 12-25. 10.1016/j.cell.2019.05.052.

Hashimoto, Y., Kinoshita, N., Greco, T.M., Federspiel, J.D., Jean Beltran, P.M., Ueno, N., and Cristea, I.M. (2019). Mechanical force induces phosphorylation-mediated signaling that underlies tissue response and robustness in Xenopus embryos. Cell systems *8*, 226-241. 10.1016/j.cels.2019.01.006.

Hernandez-Vega, A., Marsal, M., Pouille, P.A., Tosi, S., Colombelli, J., Luque, T., Navajas, D., Pagonabarraga, I., and Martin-Blanco, E. (2017). Polarized cortical tension drives zebrafish epiboly movements. The EMBO journal *36*, 25-41. 10.15252/embj.201694264.

Hino, N., Rossetti, L., Marin-Llaurado, A., Aoki, K., Trepat, X., Matsuda, M., and Hirashima, T. (2020). ERK-Mediated Mechanochemical Waves Direct Collective Cell Polarization. Dev Cell *53*, 646-660. 10.1016/j.devcel.2020.05.011.

Hnisz, D., Shrinivas, K., Young, R.A., Chakraborty, A.K., and Sharp, P.A. (2017). A Phase Separation Model for Transcriptional Control. Cell *169*, 13-23. 10.1016/j.cell.2017.02.007.

Iioka, H., Iemura, S., Natsume, T., and Kinoshita, N. (2007). Wnt signalling regulates paxillin ubiquitination essential for mesodermal cell motility. Nat Cell Biol *9*, 813-821. 10.1038/ncb1607.

Iioka, H., Ueno, N., and Kinoshita, N. (2004). Essential role of MARCKS in cortical actin dynamics during gastrulation movements. J Cell Biol *164*, 169-174. 10.1083/jcb.200310027.

Ishida, T., and Kinoshita, K. (2007). PrDOS: prediction of disordered protein regions from amino acid sequence. Nucleic Acids Res *35*, W460-464. 10.1093/nar/gkm363.

Ito, S., Okuda, S., Abe, M., Fujimoto, M., Onuki, T., Nishimura, T., and Takeichi, M. (2017). Induced cortical tension restores functional junctions in adhesion-defective carcinoma cells. Nat Commun *8*, 1834. 10.1038/s41467-017-01945-y.

Itoh, K., Ossipova, O., and Sokol, S.Y. (2014). GEF-H1 functions in apical constriction and cell intercalations and is essential for vertebrate neural tube closure. J Cell Sci *127*, 2542-2553. 10.1242/jcs.146811.

Kato, M., Han, T.W., Xie, S., Shi, K., Du, X., Wu, L.C., Mirzaei, H., Goldsmith, E.J., Longgood, J., Pei, J., et al. (2012). Cell-free formation of RNA granules: low complexity sequence domains form dynamic fibers within hydrogels. Cell *149*, 753-767. 10.1016/j.cell.2012.04.017.

Katsunuma, S., Honda, H., Shinoda, T., Ishimoto, Y., Miyata, T., Kiyonari, H., Abe, T., Nibu, K., Takai, Y., and Togashi, H. (2016). Synergistic action of nectins and cadherins generates the mosaic cellular pattern of the olfactory epithelium. J Cell Biol *212*, 561-575. 10.1083/jcb.201509020.

Kedersha, N., Ivanov, P., and Anderson, P. (2013). Stress granules and cell signaling: more than just a passing phase? Trends Biochem Sci *38*, 494-506. 10.1016/j.tibs.2013.07.004.

Kim, H.Y., and Davidson, L.A. (2013). Investigating morphogenesis in Xenopus embryos: imaging strategies, processing, and analysis. Cold Spring Harb Protoc *2013*, 298-304. 10.1101/pdb.top073890.

Kinoshita, N., Hashimoto, Y., Yasue, N., Suzuki, M., Cristea, I.M., and Ueno, N. (2020). Mechanical Stress Regulates Epithelial Tissue Integrity and Stiffness through the FGFR/Erk2 Signaling Pathway during Embryogenesis. Cell Rep *30*, 3875-3888. 10.1016/j.celrep.2020.02.074.

Konno, D., Shioi, G., Shitamukai, A., Mori, A., Kiyonari, H., Miyata, T., and Matsuzaki, F. (2008). Neuroepithelial progenitors undergo LGN-dependent planar divisions to maintain self-renewability during mammalian neurogenesis. Nat Cell Biol *10*, 93-101. 10.1038/ncb1673.

Kroschwald, S., Maharana, S., Mateju, D., Malinovska, L., Nuske, E., Poser, I., Richter, D., and Alberti, S. (2015). Promiscuous interactions and protein disaggregases determine the material state of stress-inducible RNP granules. Elife *4*, e06807.

10.7554/eLife.06807.
Leonavicius, K., Royer, C., Preece, C., Davies, B., Biggins, J.S., and Srinivas, S. (2018). Mechanics of mouse blastocyst hatching revealed by a hydrogel-based microdeformation assay. Proc Natl Acad Sci U S A *115*, 10375-10380. 10.1073/pnas.1719930115.
Li, P., Banjade, S., Cheng, H.C., Kim, S., Chen, B., Guo, L., Llaguno, M., Hollingsworth, J.V., King, D.S., Banani, S.F., et al. (2012). Phase transitions in the assembly of multivalent signalling proteins. Nature *483*, 336-340. 10.1038/nature10879.
Mimori-Kiyosue, Y., Matsui, C., Sasaki, H., and Tsukita, S. (2007). Adenomatous polyposis coli (APC) protein regulates epithelial cell migration and morphogenesis via PDZ domain-based interactions with plasma membranes. Genes Cells *12*, 219-233. 10.1111/j.1365-2443.2007.01045.x.
Murray, D.T., Kato, M., Lin, Y., Thurber, K.R., Hung, I., McKnight, S.L., and Tycko, R. (2017). Structure of FUS Protein Fibrils and Its Relevance to Self-Assembly and Phase Separation of Low-Complexity Domains. Cell *171*, 615-627. 10.1016/j.cell.2017.08.048.
Ong, J.Y., and Torres, J.Z. (2020). Phase Separation in Cell Division. Mol Cell *80*, 9-20. 10.1016/j.molcel.2020.08.007.
Otani, T., and Furuse, M. (2020). Tight Junction Structure and Function Revisited. Trends Cell Biol *30*, 805-817. 10.1016/j.tcb.2020.08.004.
Paolini, A., and Abdelilah-Seyfried, S. (2018). The mechanobiology of zebrafish cardiac valve leaflet formation. Curr Opin Cell Biol *55*, 52-58. 10.1016/j.ceb.2018.05.007.
Protter, D.S.W., and Parker, R. (2016). Principles and Properties of Stress Granules. Trends Cell Biol *26*, 668-679. 10.1016/j.tcb.2016.05.004.
Ren, Y., Li, R., Zheng, Y., and Busch, H. (1998). Cloning and characterization of GEF-H1, a microtubule-associated guanine nucleotide exchange factor for Rac and Rho GTPases. J Biol Chem *273*, 34954-34960. 10.1074/jbc.273.52.34954.
Schwayer, C., Shamipour, S., Pranjic-Ferscha, K., Schauer, A., Balda, M., Tada, M., Matter, K., and Heisenberg, C.P. (2019). Mechanosensation of Tight Junctions Depends on ZO-1 Phase Separation and Flow. Cell *179*, 937-952. 10.1016/j.cell.2019.10.006.
Shin, Y., and Brangwynne, C.P. (2017). Liquid phase condensation in cell physiology and disease. Science (New York, N.Y.) *357*. 10.1126/science.aaf4382.
Shulga, N., and Goldfarb, D.S. (2003). Binding dynamics of structural nucleoporins

govern nuclear pore complex permeability and may mediate channel gating. Mol Cell Biol *23*, 534-542. 10.1128/mcb.23.2.534-542.2003.

Shurety, W., Stewart, N.L., and Stow, J.L. (1998). Fluid-phase markers in the basolateral endocytic pathway accumulate in response to the actin assembly-promoting drug Jasplakinolide. Mol Biol Cell *9*, 957-975. 10.1091/mbc.9.4.957.

Spadaro, D., Le, S., Laroche, T., Mean, I., Jond, L., Yan, J., and Citi, S. (2017). Tension-Dependent Stretching Activates ZO-1 to Control the Junctional Localization of Its Interactors. Curr Biol *27*, 3783-3795 e3788. 10.1016/j.cub.2017.11.014.

Teng, X., Qin, L., Le Borgne, R., and Toyama, Y. (2017). Remodeling of adhesion and modulation of mechanical tensile forces during apoptosis in Drosophila epithelium. Development *144*, 95-105. 10.1242/dev.139865.

Thompson, D.W. (1917). On Growth and Form (Cambridge Univ. Press).

Vasileva, E., Sluysmans, S., Bochaton-Piallat, M.L., and Citi, S. (2017). Cell-specific diversity in the expression and organization of cytoplasmic plaque proteins of apical junctions. Ann N Y Acad Sci *1405*, 160-176. 10.1111/nyas.13391.

Wegmann, S., Eftekharzadeh, B., Tepper, K., Zoltowska, K.M., Bennett, R.E., Dujardin, S., Laskowski, P.R., MacKenzie, D., Kamath, T., Commins, C., et al. (2018). Tau protein liquid-liquid phase separation can initiate tau aggregation. The EMBO journal *37*, e98049. 10.15252/embj.201798049.

Wu, X., Cai, Q., Feng, Z., and Zhang, M. (2020). Liquid-Liquid Phase Separation in Neuronal Development and Synaptic Signaling. Dev Cell *55*, 18-29. 10.1016/j.devcel.2020.06.012.

Yamamoto, K., Miura, H., Ishida, M., Mii, Y., Kinoshita, N., Takada, S., Ueno, N., Sawai, S., Kondo, Y., and Aoki, K. (2021). Optogenetic relaxation of actomyosin contractility uncovers mechanistic roles of cortical tension during cytokinesis. Nat Commun *12*, 7145. 10.1038/s41467-021-27458-3.

Zabriskie, T.M., Klocke, J.A., Ireland, C.M., Marcus, A.H., Molinski, T.F., Faulkner, D.J., Xu, C., and Clardy, J. (1986). Jaspamide, a modified peptide from a Jaspis sponge, with insecticidal and antifungal activity. Journal of the American Chemical Society *108*, 3123-3124.

Zenker, J., White, M.D., Gasnier, M., Alvarez, Y.D., Lim, H.Y.G., Bissiere, S., Biro, M., and Plachta, N. (2018). Expanding Actin Rings Zipper the Mouse Embryo for Blastocyst Formation. Cell *173*, 776-791 e717. 10.1016/j.cell.2018.02.035.

Zhu, C., Bao, G., and Wang, N. (2000). Cell mechanics: mechanical response, cell adhesion, and molecular deformation. Annu Rev Biomed Eng *2*, 189-226. 10.1146/annurev.bioeng.2.1.189.

# Kinoshita et al. Figure 1

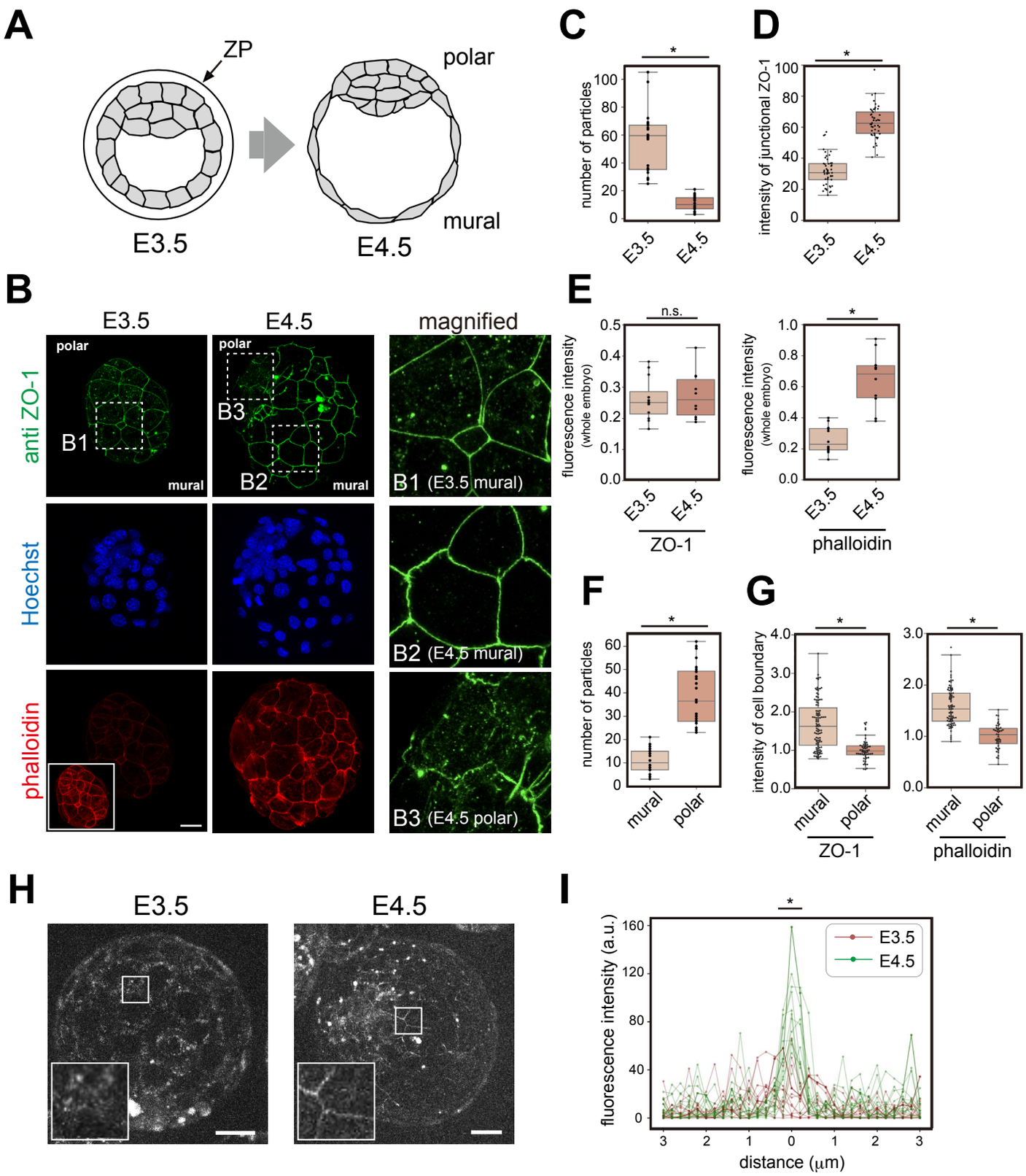

# Kinoshita et al. Figure 2

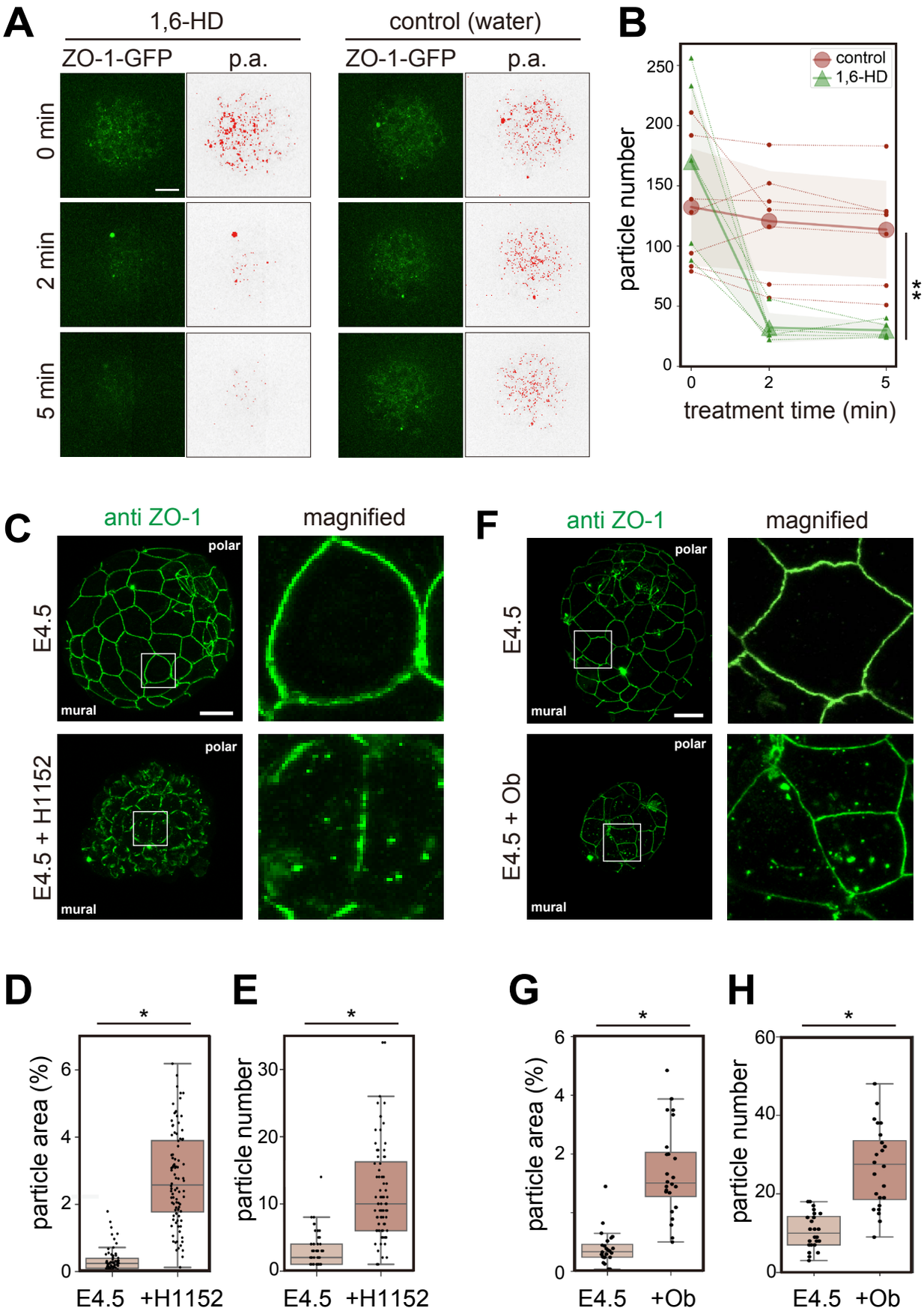

Kinoshita et al. Figure 3

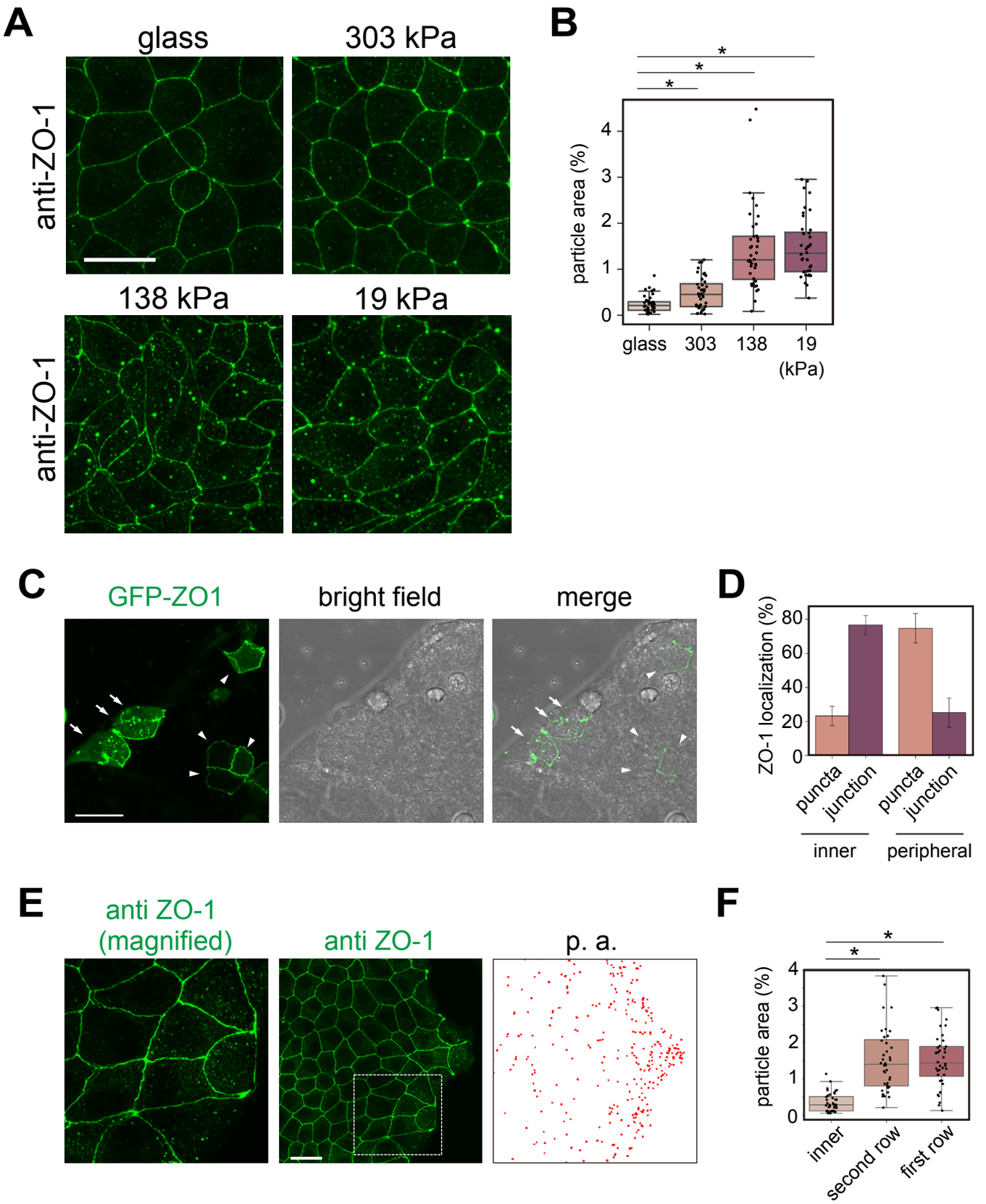

# Kinoshita et al. Figure 4

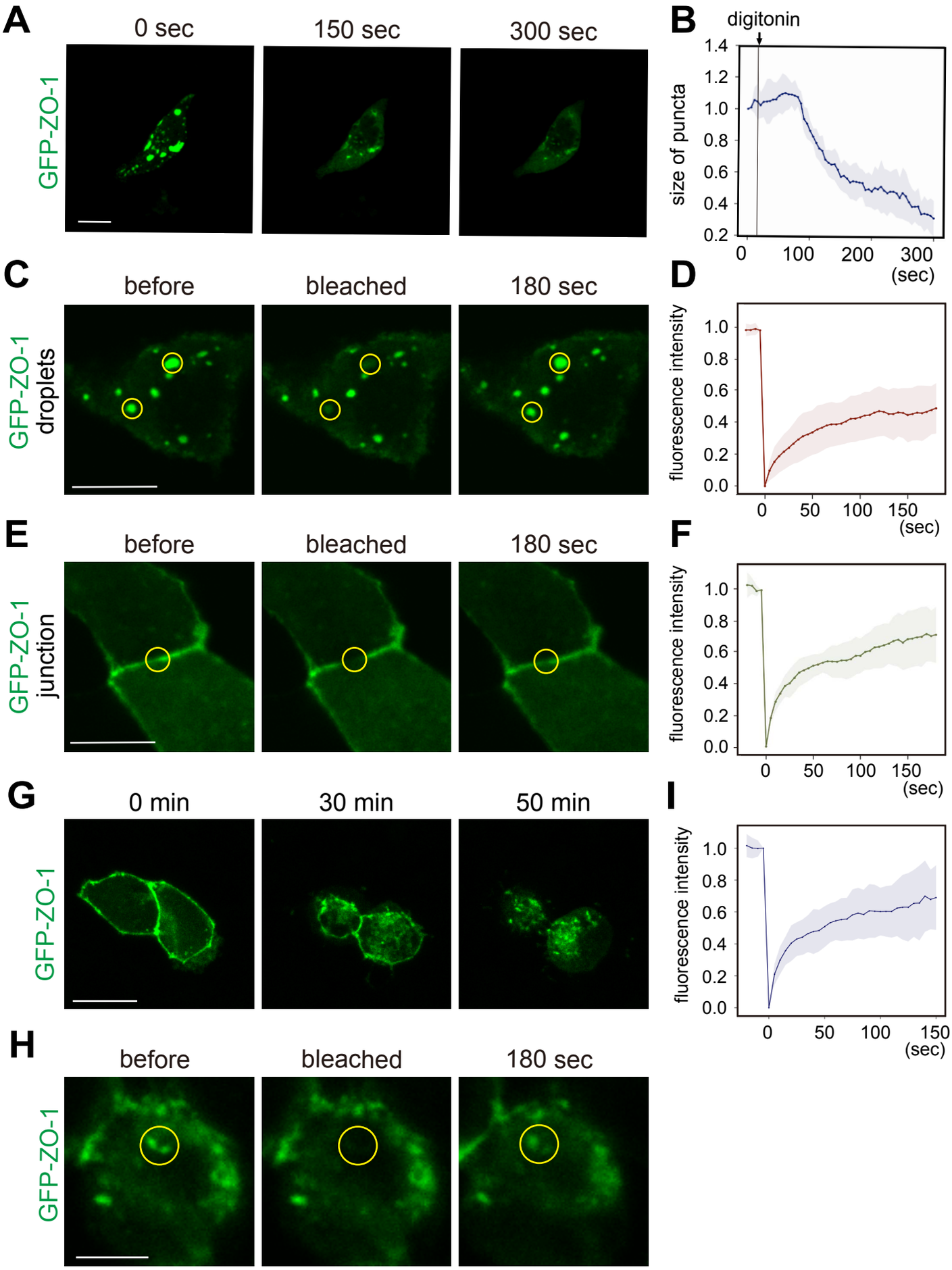

# Kinoshita et al. Figure 5

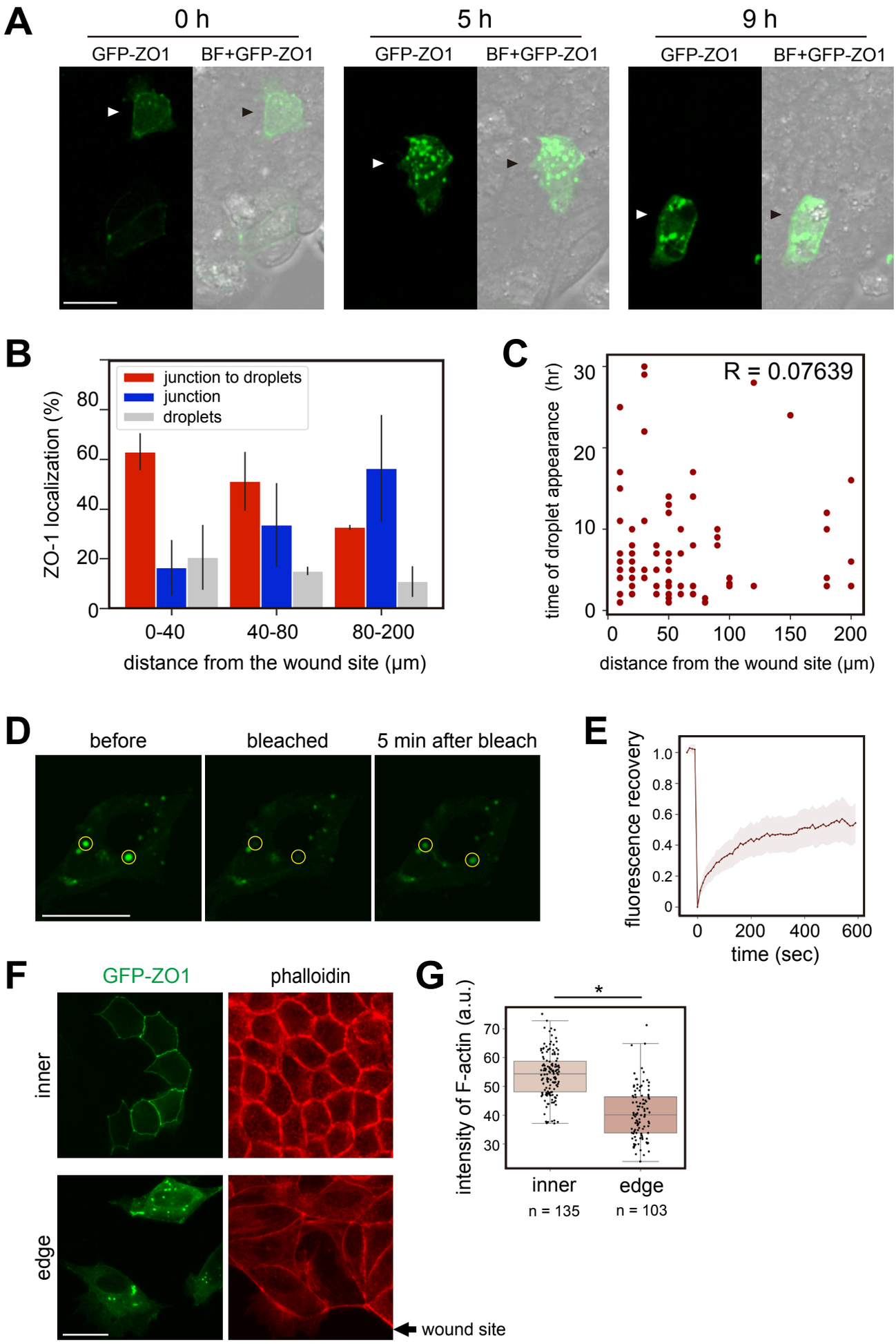
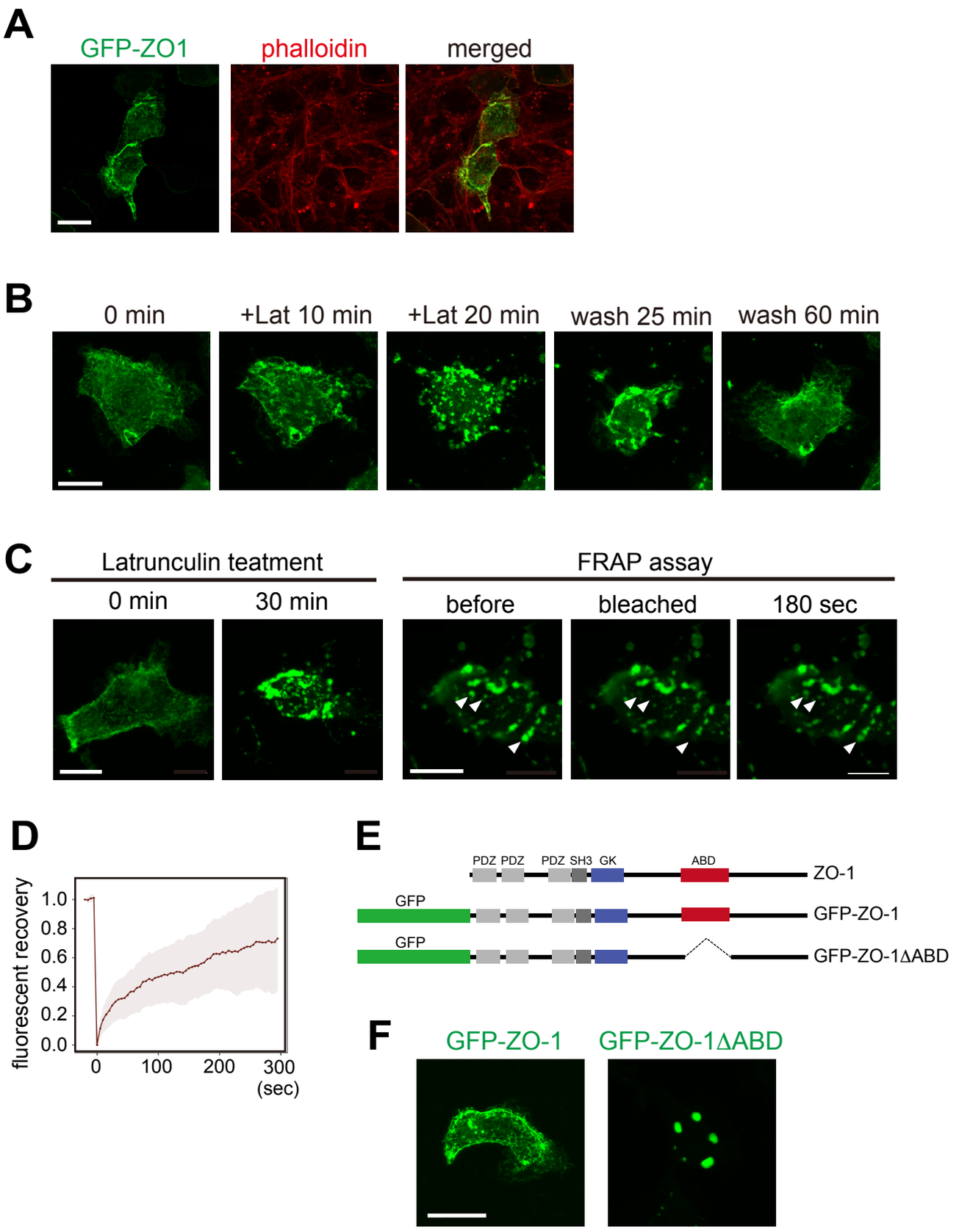
# Kinoshita et al. Figure 6